JOURNAL OF Materials CHEMISTRY

The structures and properties of hydrogen silsesquioxane (HSQ) films produced by thermal curing

Chang-Chung Yang and Wen-Chang Chen*

Department of Chemical Engineering, National Taiwan University, Taipei 106, Taiwan. Tel: 886-2-23628398; Fax: 886-2-23623040; E-mail: chenwc@ms.cc.ntu.edu.tw

Received 28th August 2001, Accepted 4th January 2002
First published as an Advance Article on the web 22nd February 2002

The structures and properties of hydrogen silsesquioxane (HSQ) films produced by curing were studied in the temperature range of 240–340 °C for various curing times. The experimental results show that the transformation of the cage structure to the network structure is the major reaction in the studied temperature range. The cage–network transformation can be explained by two-stage zero order kinetics. The rate constant of the first stage is 10–35 times more than that of the second stage. The activation energy and frequency factor of the cage–network transformation are 64.63 kJ mol^{-1} and 2.76 × 10^4 s^{-1} for the first stage while those of the second stage are 38.59 kJ mol^{-1} and 4.11 s^{-1}, respectively. The difference is probably because the network structure of the second stage limits the structural transformation and results in a small frequency factor. The porosity of the cured HSQ films increases rapidly with curing time in the first 10 min and then slowly for the remaining time. The FE-SEM (Field Emission-Scanning Electron Miscroscope) result suggests the formation of nano-pores in the cured film. The evolution of porosity is probably due to the outgassing of the reaction side-product (SiH_4), the trapped solvent (4-methylpentan-2-one) or the cage/network transformation. The last two factors contribute significantly as shown by the refractive index results of the cured films. The increasing film thickness with increasing curing time and temperature indicates the evolution of porosity in the HSQ film.

Introduction

Research interest in low dielectric constant materials for deep sub-micron IC devices remains very high.[1–5] Poly(silsesquioxane), such as hydrogen silsesquioxane (HSQ), has been recognized as a potential candidate as a low dielectric constant material.[6,7] It has a mixed cage–network structure before curing and part of the cage structure transforms to a network structure after curing as shown in Fig. 1. The dielectric,[8] mechanical,[9,10] and chemical-mechanical polishing (CMP) characteristics[11,12] of HSQ films have been reported in the literature. The properties of the HSQ films depend strongly on the curing process. Liu and Dall[8] and Liou and Pretzer[9] have demonstrated the strong dependence of the mechanical and dielectric properties of the HSQ films on the network : cage ratio at temperatures above 350 °C. Analysis of the structural changes during curing of HSQ have been reported in the literature.[13–17] The structures and reactions of HSQ films by thermal curing have been studied by Belot *et al.*,[13] Loboda *et al.*,[15] Albrecht and Blanchette,[16] and Siew *et al.*[17] There are basically four possible stages during curing of the HSQ films:

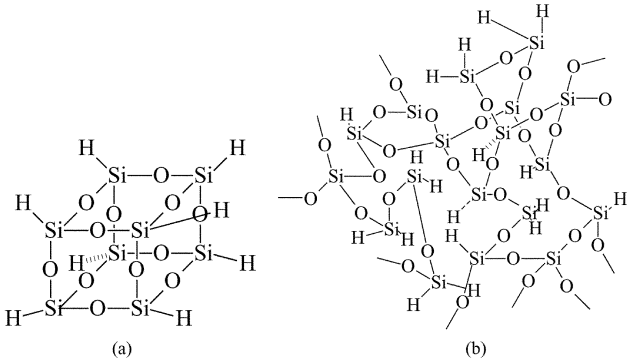

Fig. 1 Chemical structures of HSQ: (a) cage form, (b) network form.

(1) room temperature up to 200 °C: solvent loss; (2) 250–350 °C: cage–network redistribution as shown in eqn. (1a)–(1c):

$$2\,HSiO_{3/2} \rightarrow H_2SiO_{2/2} + SiO_{4/2} \quad (1a)$$

$$H_2SiO_{2/2} + HSiO_{3/2} \rightarrow SiO_{4/2} + H_3SiO_{1/2} \quad (1b)$$

$$H_3SiO_{1/2} + HSiO_{3/2} \rightarrow SiO_{4/2} + SiH_4 \quad (1c)$$

(3) 350–435 °C (or 450 °C): Si–H thermal dissociation and network redistribution as shown in eqn. (2a) and (2b):

$$4\,HSiO_{3/2} \rightarrow 3SiO_{4/2} + SiH_4 \quad (2a)$$

$$SiH_4 \rightarrow Si + 2H_2 \text{ or cleavage or } Si-H \quad (2b)$$

(4) >435 °C (or 450 °C): collapse of the pore structure. However, most of current studies focus on the structures and properties in the high temperature region of 350–500 °C. The curing mechanism of HSQ in the low temperature range of 250–350 °C was only possibly suggested by eqn. (1a)–(1c) in the literature.[16,17] The details of the reaction kinetics and the transformation of the cage structure to the network structure in the low temperature range have not been explored yet. Furthermore, a quantitative analysis of the transformation of the cage structure to the network structure is required to understand structure–property relationships. In this study, the structures and properties of HSQ films were studied when cured in the temperature range of 240–340 °C with different curing times. The studied properties included the cage–network conversion (x), refractive index, film thickness (h), and porosity (p). A kinetic model was used to simulate conversion in the studied temperature range. The rate constant, activation energy, frequency factor, and conversion of the network–cage structural transformation were also determined. FTIR was used to analyze the structural transformation and possible side reactions during curing. The variation of refractive index and porosity with curing temperatures and curing times was used to support the evidence of the structural transformation.

 DOI: 10.1039/b107697n

Experimental

Processing

The precursor, FOX-15 (solid content = 18%, solvent: 4-methylpentan-2-one), of HSQ was obtained from Dow Corning, Inc. The obtained liquid was spin-coated on four-inch wafers at 3000 rpm for 20 s. The coated films were then cured on a hot-plate under a hood in the temperature range 240–340 °C and characterized at curing times of 0, 0.5, 1, 2, 3, 4, 5, 10, 15, 20, 30, 40, and 60 min.. The structural transformation and property variation changed rapidly initially and thus more data points were taken initially.

Characterization

The chemical structure of the cured films on wafers was characterized by Fourier Transform Infrared (FTIR) spectrophotometry using a JASCO FT/IR-410 module. The transformation from the cage structure to the network structure was monitored through the variation of the peak area of the 1070 cm^{-1} peak and the 1130 cm^{-1} peak. By subtracting the peak area of the Si–O–Si network band at curing time $t = 0$ from that at $t = t$, the conversion (x) at each curing temperature and curing time was defined as in eqn. (3) in which $v_{1070\ cm^{-1}}$ and $v_{1130\ cm^{-1}}$ represented the areas of the 1070 cm^{-1} and 1130 cm^{-1} absorption peaks, respectively.

$$x(t) = \left(\frac{v_{1070\ cm^{-1}}}{v_{(1070\ cm^{-1}\ +\ 1130\ cm^{-1})}}\right)_t - \left(\frac{v_{1070\ cm^{-1}}}{v_{(1070\ cm^{-1}\ +\ 1130\ cm^{-1})}}\right)_{t=0} \quad (3)$$

The refractive index and the film thickness (h) of the cured films on wafers were then measured using a GAERTNER L116D ellipsometer (GAERTNER Scientific Co.). The porosity (p) of the cured HSQ film was determined by the effective medium approximation (EMA) module of the ellipsometer (module: VB-200, J. A. Wollam Co.). Normalized film thickness h_n shown in eqn. (4) was defined as the difference between the value at time t (h_t) and the minimum value (h_{min}) divided by h_{min}. Normalized porosity p_n shown in eqn. (5) was defined as the difference between the value at time t (p_t) and that at time zero ($p_{t\ =\ 0}$). Normalization was used to eliminate the difference in the initial structures and properties for each sample before curing.

$$h_n = \frac{h_t - h_{min}}{h_{min}} \quad (4)$$

$$p_n = p_t - p_{t=0} \quad (5)$$

Scanning electron microscopy using an Hitachi S-4000 instrument (Hitachi, Ltd.) was used to obtain electron micrographs of the cross-section of the HSQ films.

Results and discussion

Fig. 2 shows the FTIR absorption peaks at 1070 and 1130 cm^{-1} of the HSQ films cured at 300 °C at different curing times. The peak intensity at 1070 cm^{-1} increases with increasing curing time while the peak at 1130 cm^{-1} shows a reverse trend. Note that the peaks at 1070 and 1130 cm^{-1} represent the network and cage structures of the HSQ films, respectively.[15,16] Hence, the structural transformation from the cage structure to the network structure at 300 °C increases with curing time. Fig. 3 illustrates the intensity increasing in the FTIR bands at 981 and 946 cm^{-1} with curing times at 300 °C. These two bands are assigned to the formation of $H_2SiO_{2/2}$ from $HSiO_{3/2}$.[18,19] Therefore, eqn. (1a): $2\,HSiO_{3/2} \rightarrow H_2SiO_{2/2} + SiO_{4/2}$ is the major reaction responsible for the chemical reaction that occurred at 300 °C. The FTIR spectra of the HSQ films cured at other temperatures also show a similar behavior as that at 300 °C.

Fig. 4 shows the variation of the structural conversion (x) of the HSQ thin films with curing temperatures from 240 to 340 °C and curing times from 0 to 60 min. A two-stage structural conversion is observed for each curing temperature in this figure. The conversion increases rapidly in the first 10 min and then slowly increases to 60 min. This result suggests that the cage structure of the HSQ films transforms to the network structure during thermal curing. The cage–network transformation can be explained by a two-stage zero order kinetic model since the self-structural transformation occurs during curing. Fig. 5 shows the variation of the rate constants with the inversion of curing temperatures by the Arrhenius equation for the first and second stages. The rate constant of the first stage is 10–35 times more than that of the second stage. The activation energy and frequency factor for the network–cage transformation are 64.63 kJ mol^{-1} and 2.76 × 10^4 s^{-1} for the first stage while those of the second stage are 38.59 kJ mol^{-1} and 4.11 s^{-1}.

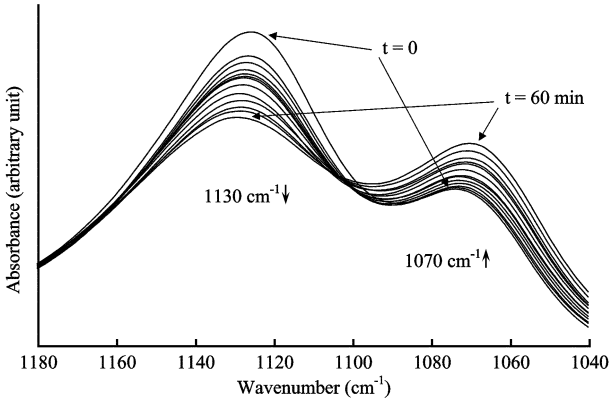

Fig. 2 FTIR spectrum of the HSQ thin film cured at 300 °C for different times from as-spun to 60 min.

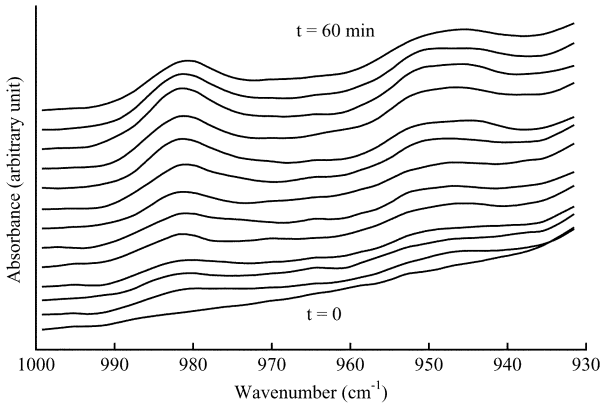

Fig. 3 Variation of the FTIR bands at 981 and 946 cm^{-1} with curing times at the curing temperature of 300 °C.

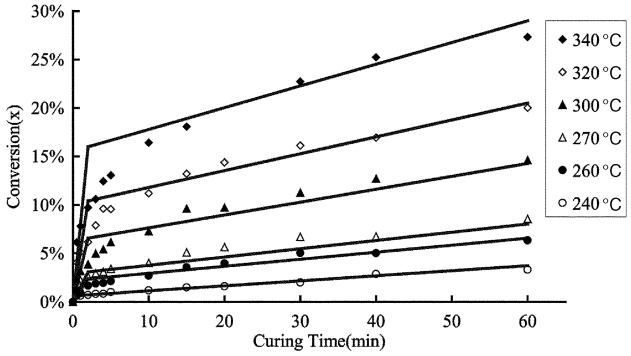

Fig. 4 Variation of the conversion (x) with curing times of 0–60 min at curing temperatures of 240, 260, 270, 300, 320, and 340 °C.

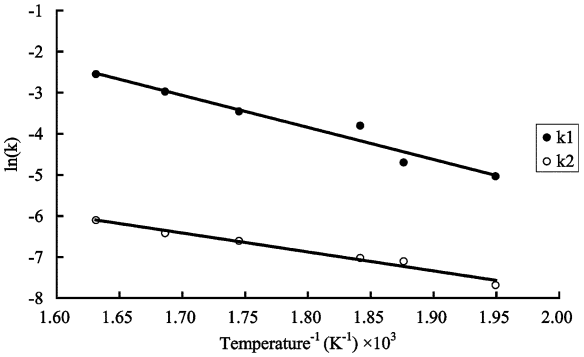

Fig. 5 Variation of the rate constants (units: s^{-1}) for the first (k_1) and second stages (k_2) with the inverse of the curing temperatures (units: K^{-1}).

Sabin and Albrecht[20] also reported a similar activation energy of 65.60 kJ mol^{-1} for the first stage. Albrecht and Blanchette[16] reported the activation energy of 57.88 kJ mol^{-1} for HSQ curing in the first five minutes, which is close to the activation energy of the first stage. However, the second stage curing kinetics are not observed in their study. The activation energy of the second stage is comparable with that of the first stage. However, the frequency factor is four orders of magnitude smaller than that of the first stage. This is probably because the network structure of the second stage limits the structural transformation.

Fig. 6 shows the variation of the (Si–H/Si–O–Si) peak ratio with conversion (x) for different curing temperatures. The (Si–H/Si–O–Si) peak ratio was calculated from the area of the peak at 2250 cm^{-1} (Si–H vibration[7,15,16,18]) divided by the peak area of 1070 + 1130 cm^{-1} (Si–O–Si network and cage structures). For curing at 240, 260, and 270 °C, the peak ratio remains almost constant at different conversions. However, the peak ratio starts to decreases at 300 °C and drops rapidly at 340 °C. It is possible that Si–H bond cleavage [eqn. (2b)] probably occurs in the temperature range of 300–340 °C. Loboda *et al.*[15] have shown that the oxidation of SiH_4 does not occur below 340 °C. Thus, it does not play a significant role in the structures and properties of the HSQ films under the studied temperature range.

The structures and properties of the cured HSQ films were significantly modified by thermal curing. The FE-SEM (Field Emission-Scanning Electron Microscopy) diagram of the HSQ film curing at 300 °C for 60 min is shown in Fig. 7. It can be seen that a substantial number of nanoscale pores exist in the cured HSQ film, which do not exist in the initial cured HSQ film. Fig. 8 shows the variation of porosity (p_n) and film

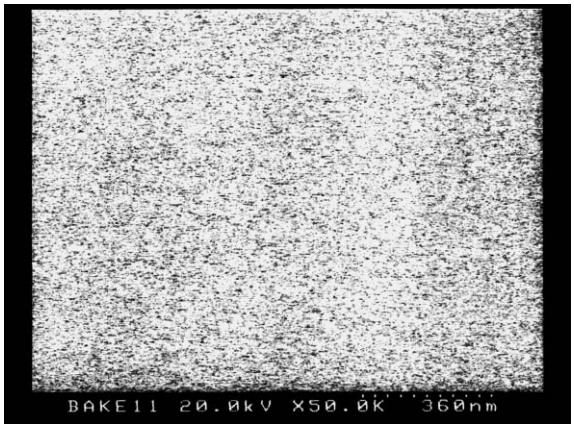

Fig. 7 FE-SEM diagram of the HSQ film cured at 300 °C for 60 min.

thickness (h_n) with different curing times at a curing temperature of 300 °C. The porosity increases by about 2% for a curing time of 60 min while the film thickness increases by 2.5%. The increase in film porosity results in an increase in the film thickness. The initial drop of the film thickness (vertical line) in Fig. 8 is due to the evaporation of the solvent, 4-methylpentan-2-one. There are three possibilities for the increase of the film porosity. One is outgassing of the side products during thermal curing. The other possibility is that the solvent trapped in the films comes out of the films during thermal curing. $H_2SiO_{2/2}$ of eqn. (1a) can be further decomposed to SiH_4 and H_2 by thermal treatment, as shown in eqn. (1b), (1c) and (2b). As SiH_4 escapes from the HSQ films, it is possible for the formation of the film porosity. Siew *et al.*[17] also observed the decomposition of the trapped solvent and the side products SiH_4 and H_2 by TGA, which provides further support for the present study. The cage–network transformation also contributes to the variation of film porosity. Note that the cage structure of HSQ allows a denser packing than the random structure and results in the variation of film porosity.

Fig. 9 shows the variation of the refractive index of the film with curing temperatures and curing times. The refractive index at a curing time of 60 min decreases from 1.388 to 1.369 as the curing temperature increases from 240 to 340 °C, as shown in this figure. For each curing temperature, the refractive index drops rapidly in the first 10 min and remains almost constant for the next 50 min. The refractive index is related to the molecular composition and free volume. As shown in Fig. 4 and 8, the conversion and film porosity change significantly in the first 10 min and slowly for the next 50 min. It explains the refractive index profile shown in Fig. 9. At curing temperatures of 240, 260, and 270 °C, there is no significant compositional

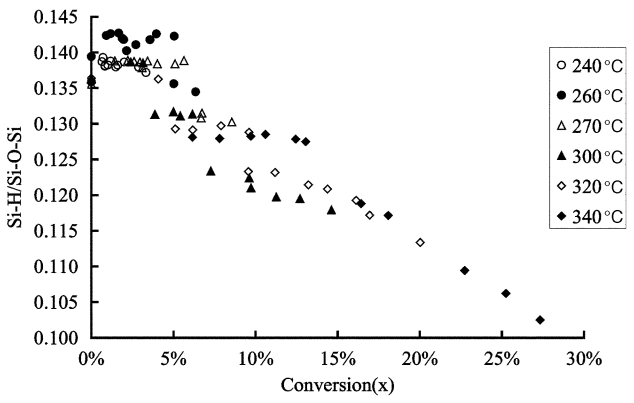

Fig. 6 Variation of (Si–H/Si–O–Si) FTIR peak ratios with the corresponding conversion at curing temperatures of 240, 260, 270, 300, 320, and 340 °C.

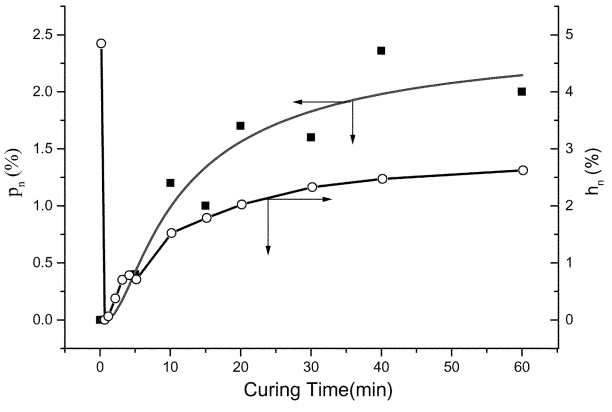

Fig. 8 Variation of the normalized film porosity (p_n) and film thickness (h_n) of the HSQ thin films with different curing times at the curing temperature of 300 °C.

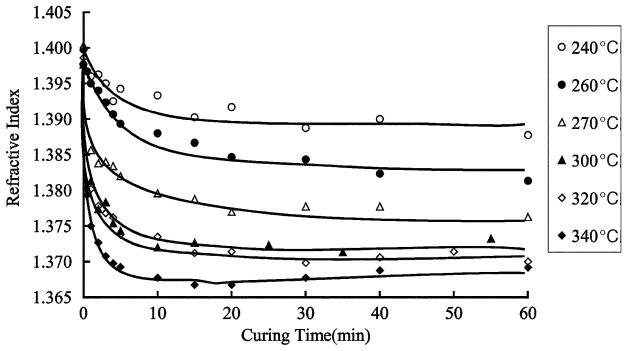

Fig. 9 Variation of the refractive index of the HSQ films with different curing temperatures and curing times.

change from Fig. 6. Thus, the decrease in refractive index is probably due to an increase in free volume. The variation of the free volume is probably due to the outgassing of the trapped solvents or the transformation of the cage–network structure. At curing temperatures of 300 °C and above, Si–H bonding decreases greatly with increasing curing time from Fig. 6. However, the refractive index changes insignificantly after a curing time of 10 min. It suggests that the compositional variation from the dissociation of the Si–H bond contributes insignificantly to changes in the refractive index. Furthermore, the film porosity changes rapidly in the initial curing stage and then reaches a steady value. Hence, the refractive index profile shown in Fig. 9 is mostly dependent on the film porosity caused by the outgassing of the trapped solvents or the cage–network transformation in the studied temperature range.

Conclusions

A two-stage zero order kinetic model has been developed to explain the network–cage transformation of HSQ films cured in the temperature range of 240–340 °C. The rate constant in the first stage is much larger than that in the second stage. This is probably because the network structure of the second stage limits structural transformation and results in a small frequency factor. The porosity of the cured HSQ films increases rapidly in the initial curing stages and then slowly for the remaining time. The FE-SEM result suggests the formation of nano-pores in the cured film. The evolution of porosity is probably due to outgassing of the reaction side-product (SiH_4), trapped solvent or the cage–network transformation. The last two factors dominate the formation of porosity and the variation of refractive index in the cured films.

Acknowledgements

The authors thank the National Science Council of Taiwan for financial support of this work and the Dow Corning Co. for providing the Fox-15 samples. The support of National Nano Device Laboratories (Hsinchu, Taiwan) under contract NDL 90-C-037 is also highly appreciated.

References

1 *Low-Dielectric Constant Materials – Synthesis and Applications in Microelectronics*, T. M. Lu, S. P. Murarka, T. S. Kuan and C. H. Ting, ed., The Materials Research Society, Pittsburgh, PA, 1995, vol. 381.
2 *Low-Dielectric Constant Materials II*, A. Lagendijk, H. Treichel, K. J. Uram and A. C. Jones, ed., The Materials Research Society, Pittsburgh, PA, 1996, vol. 443.
3 *Low-Dielectric Constant Materials III*, C. Case, P. Kohl, T. Kikkawa and W. W. Lee, ed., The Materials Research Society, Pittsburgh, PA, 1997, vol. 476.
4 *Low-Dielectric Constant Materials IV*, C. Chiang, P. S. Ho, T. M. Lu and J. T. Wetzel, ed., The Materials Research Society, Warrendale, PA, 1998, vol. 511.
5 *Low-Dielectric Constant Materials V*, J. Hummel, K. Endo, W. W. Lee, M. Mills and S. Q. Wang, ed., The Materials Research Society, Warrendale, PA, 1999, vol. 565.
6 M. J. Loboda and G. A. Toskey, *Solid State Technol.*, 1998, **41**, 99.
7 J. N. Bremmer, Y. Liu, K. G. Gruszynski and F. C. Dall, in ref. 3, p. 37.
8 Y. Liu and F. Dall, in ref. 5, p. 267.
9 H. C. Liou and J. Pretzer, *Thin Solid Films*, 1998, **335**, 186.
10 R. F. Cook and E. G. Liniger, *J. Electrochem. Soc.*, 1999, **146**, 4439.
11 W. C. Chen, S. C. Lin, B. T. Dai and M. S. Tsai, *J. Electrochem. Soc.*, 1999, **146**, 3004.
12 W. C. Chen and C. T. Yen, *J. Polym. Res.*, 1999, **6**, 197.
13 V. Belot, R. Corriu, D. Leclercq, P. H. Mutin and A. Vioux, *Chem. Mater.*, 1991, **3**, 127.
14 D. Tobben, P. Weigard, M. J. Shapiro and S. A. Cohen, in ref. 2, p. 195.
15 M. J. Loboda, C. M. Grove and R. F. Schneider, *J. Electrochem. Soc.*, 1998, **145**, 2861.
16 M. G. Albrecht and C. Blanchette, *J. Electrochem. Soc.*, 1998, **145**, 4019.
17 Y. K. Siew, G. Sarkar, X. Hu, J. Hui, A. See and C. T. Chua, *J. Electrochem. Soc.*, 2000, **147**, 335.
18 P. Bornhauser and G. Calzaferri, *J. Phys. Chem.*, 1996, **100**, 2035.
19 D. Seyferth, C. Prud'homme and G. H. Wiseman, *Inorg. Chem.*, 1983, **22**, 2163.
20 E. Sabin and G. Albrecht, The Electrochemical Society Meeting Abstract, vol. 97-1, Montreal, Quebec, Canada, May 4–9, 1997, abstract 256, p. 320.